

A single photon detection system for visible and infrared spectrum range

Alexander Divochiy,* Yury Vakhtomin, and Pavel Morozov

*LLC SCONTEL, 5/1-14 L'va Tolstogo st, Moscow 119021, Russian Federation and
Moscow State University of Education (MSPU), 1/1 M. Pirogovskaya st., Moscow 119991, Russian Federation*

Konstantin Smirnov and Philipp Zolotov

*LLC SCONTEL, 5/1-14 L'va Tolstogo st, Moscow 119021, Russian Federation
Moscow State University of Education (MSPU), 1/1 M. Pirogovskaya st., Moscow 119991, Russian Federation and
National Research University Higher School of Economics, Moscow 101000, Russian Federation*

Marta Misiaszek* and Piotr Kolenderski†

Faculty of Physics, Astronomy and Informatics, Nicolaus Copernicus University, Grudziadzka 5, 87-100 Toruń, Poland

We demonstrate niobium nitride based superconducting single-photon detectors sensitive in the spectral range 452 nm – 2300 nm. The system performance was tested in a real-life experiment with correlated photons generated by means of spontaneous parametric down conversion, where one of photon was in the visible range and the other was in the infrared range. We measured a signal to noise ratio as high as 4×10^4 in our detection setting. A photon detection efficiency as high as 64% at 1550 nm and 15 % at 2300 nm was observed.

I. INTRODUCTION

Recent advances in field of the superconducting single-photon detectors (SSPD) have introduced many conceptual ideas which allow us to progress their capabilities. Specifically, quantum efficiency (QE) of SSPDs and system detection efficiency (SDE) of SSPD-based systems have been increased to near-unity values at telecom wavelength range[1–5]. The timing resolution can reach values below 17.8 ps [6], which is inaccessible for other single-photon detection technologies, such as silicon and In-GaAs/InP photodiodes. In addition to that, SSPDs are considered to be the only available type of the single-photon detectors capable of operation in the wide spectral range, starting from near-UV [7]up to mid-IR [8–11] wavelengths. On the other hand, the small size of SSPDs makes it challenging to couple photons to its sensitive area. Typically, it requires single-mode fibers mounted directly to SSPD.

As it is known, SDE of SSPDs depends on two quantities, the absorption and the intrinsic quantum efficiency. The absorption depends on the properties of optical structures, incident field and photon coupling with sensitive area of a detector. The intrinsic quantum efficiency is meant as the probability of resistive state formation due to an absorption event. It depends on the characteristics of the superconducting film. Both the parameters should be maximized in order to make SDE as high as possible. The former can be maximized by proper optical cavity fabrication and can reach near-unity values at particular narrow wavelength range. On the other hand, the optimization of the intrinsic quantum efficiency is a more complexed task. It is higher at lower working tempera-

ture [8, 11] and for narrow superconducting stripes [9], as for the materials with lower superconductor energy gap of superconducting material. However, the limits of the gap are dictated by the device operating temperature.

The very first implementation of SSPD with single-mode fluoride fiber input showed SDE below 1% at 2200 nm [12]. The detectors were cooled in liquid He₄ down to 1.7K. More recently the use of multi-mode chalcogenide fiber (IRF-S-100) for transmission of MID-IR photons allowed detection of photons in the range up to 7 μm [10]. However, due to the mismatch in size between the fiber core and the detector only 1% of the light incident on the fiber input reached the SSPD. As a material for fabrication of superconducting structure WSi was used. It has a lower critical temperature as compared to niobium nitride (NbN) so it can potentially be more useful for mid-IR applications. This is the price of having a working temperature in sub-Kelvin range.

In our work, we show that the single photon detecting system with NbN-based SSPDs, single-mode fibers and Gifford-McMahon cryocooler (Sumitomo RDK-101D), reaches characteristics which are superior to all previously published such systems for the wavelength range up to 2300 nm. In order to increase the intrinsic quantum efficiency of the detectors, we used an approach similar to the one presented earlier [13], which allows us to fabricate disordered NbN films. In our previous work [14] we presented preliminary tests of detectors optimized for the 1600 – 2200 nm range. In addition, it was calculated that in the mid-IR wavelength region the intrinsic quantum efficiency of the device could be as high as 10%. Presented coupling schemes could not find their place in the routine experiments because they imply significant prevalence of black body radiation over the signal of interest. To investigate exact values of the SDE of SSPD in the spectrum range up to 2300 nm we suggest two main novelties with respect to the detector systems used in the telecom range. An optimized solution for the cou-

* These authors contributed equally to this work.

† kolenderski@fizyka.umk.pl

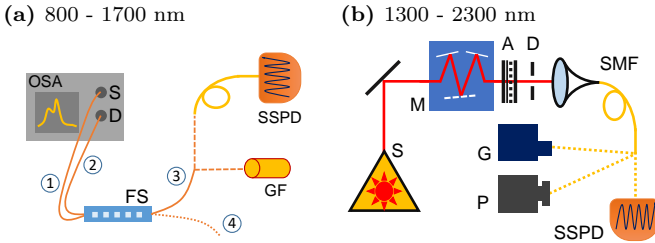


FIG. 1. Absorption measurement setups. For the range of (a) 800 – 1700 nm: OSA – Optical Spectrum Analyzer (Keysight HP 70950A), S – radiation source, D – detector, FS – 50:50 fiber splitter for 1550 nm, GF – gold-tip ferule, SSPD (b) 1300 – 2300 nm: S – photon source (xenon lamp), M – monochromator, A – attenuator, D – diaphragm, detectors: G – Golay cell, P – power meter (Ophir PD-300 IRG), SSPD.

pling scheme requires the use of SMF2000 single-mode fiber with the NbN devices. This significantly increases the allowed operation temperature of the system, which is possible to reach in a typical close-cycle cryostat.

II. SSPD CHARACTERIZATION

We used our standard technique [13, 14] for fabrication of the devices analysed here. The aim was to get higher absorption above 1550 nm which was done by thickening the dielectric Si_3N_4 layer. This layer has a refractive index of 2.3 and a thickness of 185 nm. We begin with the analysis of the absorption of our devices as a function of incident photon wavelength.

We investigate the absorption for the spectral range of 800 – 2300 nm. It has been done in two steps by using two measurement apparatus depicted in Fig. 1: (a) first for the range of 800 – 1700 nm and (b) the other one for the range of 1300 – 2300 nm.

For the analysis of the spectral absorption of our structures we used an optical spectrum analyzer (OSA) with built-in broadband radiation source allowing for measurement in the spectral range of 800 – 1700 nm, see Fig. 1(a). We used a fiber splitter (50:50 distribution at 1550 nm) for simultaneous illumination and detection of the absorption and reference spectrum. The broadband light source was connected to port number 1 and OSA monitored the output port 2. Port number 3 was connected to either gold mirror or SSPD under the study. The reflected light was sent back and registered by OSA. Port number 4 of the splitter was not used. The fiber splitter's partition coefficient is wavelength-dependent and therefore in order to perform absorption measurements of superconducting structures, the reference spectra with a gold mirror was acquired. We deposited 100 nm thick gold layer on the standard ferule to make sure that there is no air gap between the gold mirror and the fiber port 3. Thanks to that, in the scheme with SSPD detector,

we could calculate the absolute values of the absorption.

The measured spectra $P = P(\lambda)$ on port 2 of the fiber splitter, FS, see Fig. 1, in the case of SSPD and gold-tip ferule, GF, are $P_{\text{SSPD}}(\lambda) = T_{\text{BS}}^2 R_{\text{SSPD}} \cdot P_0(\lambda)$ and $P_{\text{GF}}(\lambda) = T_{\text{BS}}^2 R_{\text{GF}} \cdot P(\lambda)$, respectively. Here $P(\lambda)$ is the light source spectrum, T_{BS} is the transmission coefficient of the fiber splitter and $R_{\text{SSPD}}, R_{\text{GF}}$ are the reflection coefficients of the superconducting structures and gold-tip ferule. Assuming the perfect reflection from the gold mirror (GF), we can put $R_{\text{GF}} = 1$. As a result, we get the relation $P_{\text{SSPD}}/P_{\text{GF}} = R_{\text{SSPD}}$. By definition, the absorption coefficient reads $A_{\text{SSPD}} = 1 - R_{\text{SSPD}}$, so finally one gets $A_{\text{SSPD}} = 1 - P_{\text{SSPD}}/P_{\text{GF}}$. The measured absorption is depicted in Fig. 2 with a blue curve.

In order to investigate SDE above 1700 nm, another measurement technique was developed. It is presented in Fig. 1 (b). The experimental setup was based on an IR spectrophotometer (IKS-19). Light from the xenon lamp was led to the single diffraction grating with 300 grooves/mm. The output slit of 1 mm width defines 5 nm bandwidth of the output radiation. Next, the radiation is attenuated by a set of 1-inch Si wafers with deposited thin NbN films of thicknesses 5, 10, 20 and 30 nm and transmittance of 0.4, 0.1, 0.03 and 0.01, respectively. After the attenuator, we used a 0.5 mm diaphragm and the SM2000 single-mode fiber to collect free-space radiation.

Due to the fact that transmittance of attenuators depends on wavelength, we calibrated each of them on each wavelength of interest by measuring power with and without attenuation. In order to measure power, we used Golay cell (Tydex, GS-1D [15]), which has 6 mm diameter input covered by diamond window. Furthermore, it has noise equivalent power $\text{NEP} = 10^{-9} \text{ W} \cdot \text{Hz}^{-\frac{1}{2}}$, which does not vary in spectral range of interest. As a result, it perfectly meets the requirements of our experiment. In order to use Golay cell as a power meter we measured its responsivity, which was estimated to be 6800 V/W. The responsivity measurement was performed using 1550 nm diode laser and a power meter (Ophir, PD-300 IRG). In order to define the part of the optical power, which can be collected to the single-mode fiber, we measured power at the fiber output directly with the power meter in the range of 1310 – 1600 nm. The power meter accuracy is 1 pW in this spectral range. By comparing these results with those achieved on the output of the monochromator with the Golay cell we found that the coupling coefficient is equal to 0.0189(8). We assume this coefficient to be constant for the spectral range of 1310 – 2300 nm.

For the measurements, the target power of 0.5 – 2 pW was adjusted using a set of attenuators. Single mode fiber, SM2000, was connected to the optical input of the SSPD. The SDE was calculated by measuring the number of electrical pulses using an universal frequency counter (Agilent, A53131). The results of the experiment are presented in Fig. 2 with purple triangles. Note, the difference between the SDE for polarized and unpolarized light stems from the meander-type geometry of the SSPD

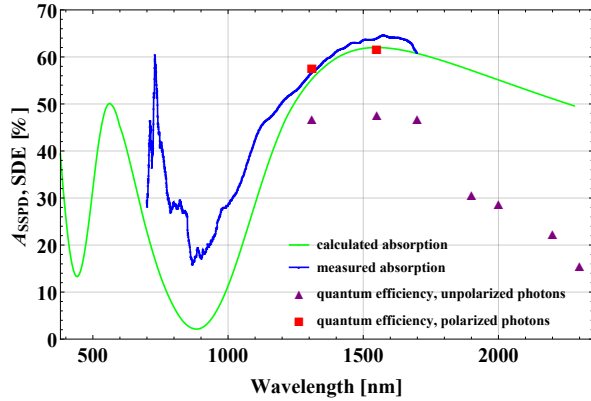


FIG. 2. The spectral absorption, A_{SSPD} , and system detection efficiency, SDE.

[16, 17]. The system detection efficiency at 1310 nm and 1550 nm was approximately 0.45. Then efficiency decreases with decreasing photon energies. In order to estimate the maximal SDE values we also measured quantum efficiency with a linearly polarized light source at available wavelengths. In this case the best values for our detectors were 0.58 and 0.62 at 1310 nm and 1550 nm, respectively.

A. Simulation of absorption in the range of 380 – 2300nm

In our work spectral simulations of absorption for the range of 380 – 2300 nm were performed with OpenFilters software [18]. We adopted parameters of our sample from previous work[16]. Note that the optical properties of thin NbN films vary[16, 19], which could be explained by differences in stoichiometry of the films. The absorption coefficient was calculated for unpolarized radiation incident on a Au/Si₃N₄/NbN structure (80 nm/185 nm/5 nm thick respectively) from SiO₂ medium. In our simulation we assume that the film is uniform, because the etched regions are much smaller than the wavelengths. The NbN meander pattern with filling factor of 0.5 is ignored. The green curve in Fig. 2 presents the simulated absorption spectral dependence for the superconducting structure. A fair agreement between the measured and simulated characteristics in the region of 1300 – 1700 nm confirms the accuracy of our back-reflection method, which justifies its application for future spectral data analysis.

III. APPLICATION FOR CORRELATED PHOTON PAIRS

A. Experimental setup

Finally, we tested our SSPDs with a correlated photon source based on the process of spontaneous parametric

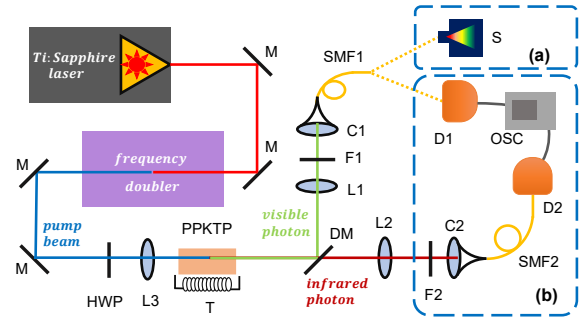


FIG. 3. Experimental setup. Pulsed Ti:Sapphire laser, M – mirror, L3 – lens (focal length $f = 10$ cm), PPKTP – periodically poled potassium titanyl phosphate crystal, T – temperature controller, DM – dichroic mirror (Semrock 76-875 LP), L1, L2 – plano-convex lens ($f = 12$ cm, 15 cm), F1 – set of filters (three settings: (1) Chroma ET500 and Z532-rdc, (2) 2 pcs of AHF 442 LP, (3) 2pcs of AHF 442 LP and Thorlabs FESH0700), C1,C2 – single mode fiber coupler ($f = 0.8$ cm, 1.51 cm), F2 – long-pass filter (Semrock BLP01-1319R), SMF1, SMF2 – single mode fiber (two settings: (1) Thorlabs SMF460B and SMF1550, (2) SMF780 and SMF2000) Detection setups: a) S – spectrometer (Ocean Optics USB2000+), b) D1, D2 – detectors, OSC – oscilloscope.

down conversion (SPDC), which we use to investigate their performance in correlation-type measurements[20, 21]. The experimental setup is depicted in Fig. 3. A frequency doubled tunable Ti:Sapphire laser pumps the photon pair source based on a periodically poled potassium titanyl phosphate (PPKTP) crystal. The photons are coupled into single mode fibers. The spectra of the output photons can be modified by tuning the pump photon spectrum. The pump beam is tuned in the range of 377 – 404 nm. It allows for generation of pairs of photons, where one photon is in 452 – 575 nm spectral range and the other one in the 1363 – 2299 range. The measured tuning curve is presented in Fig. 4. The pump and visible photon spectra are analyzed using a spectrometer. The spectrum of the infrared photon is calculated based on the energy conservation relation.

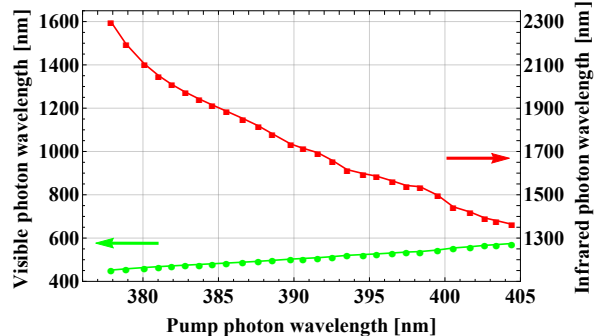


FIG. 4. Generated photon wavelengths. Green dots show measured wavelengths of visible photon, red one are calculated from energy conservation relation.

B. Results

The coincidence measurements are performed using three types of detectors: 1) SSPD: bias current $21\mu\text{A}$, 2) InGaAs/InP, detection efficiency 10%, gate width 20 ns, deadtime $10\ \mu\text{s}$, and 3) silicon avalanche photodiode (Si APD). The output signals from the detectors are then analyzed using an oscilloscope, Fig. 3(b). The timing histogram of the relative pulse arrival times are measured. The data set consists of 10^4 samples. Figure Fig. 5(a) shows examples of measurement results for different pairs of detectors: a) Si APD and InGaAs/InP, b) Si APD and SSPD and c) two SSPDs.

The coincidence counting measurement results, as seen in Fig. 5 (a), allow us to estimate the signal to noise ratio (SNR) by fitting the Gaussian function $b + a \exp[-4 \ln 2 (t - t_0)^2 / \sigma^2]$ to the timing histograms. In our model b stands for the background noise, a is the signal amplitude, σ is the timing jitter and t_0 is the time where the pick maximum value occurs. Based on this definition $\text{SNR} = a/b\sqrt{\pi/16\log(2)}\text{erf}(2\sqrt{\log(2)}) \approx 0.52a/b$.

The SNR results are gathered in panel (b) in Fig. 5. We compare SSPDs with InGaAs/InP detectors in the exactly the same settings (F1 filter setting 1 and fibers setting 1 as described in caption of Fig. 3). The results are depicted with green diamonds and orange squares. One can clearly see the limit around 1650 nm beyond which the InGaAs/InP detector quantum efficiency drops to zero. The dark count rate of our Si APD was around 3 kcps, which originated in an intrinsic dark counts of the detector itself and stray light. The typical Si APDs' noise is around 100 cps. Therefore, in principle, it is expected that SNR can increase in that case by one order of magnitude. Moreover, one can observe a plateau in the range 1900 – 2200 nm, which we attribute to the interplay of SDE for visible and infrared photons.

Next, we use two SSPD detectors with different filters (F1 filter as denoted in setting 2 in Fig. 3). The measurement results are marked using red triangles. This filter allows us to investigate the system performance in the broad range of wavelengths up to 2151 nm. One can also see the improved SNR by approximately one order of magnitude. In the following step the SNR was improved by approximately 2 orders of magnitude by replacing the fibers (setting 2) and filters (setting 3). This allowed us to broaden the spectral range even further. It should be noted that in the range 1900 – 2300 nm the SSPDs efficiency drop can be explained by small photon energies.

Recently, in the Ref. [5] we experimentally showed that the fabrication of SSPD detectors based on structurally disordered films [22–25] allows for saturated dependence of the detection efficiency at lower bias current. This is based on the observation that the critical temperature and the electron diffusion coefficient follow the trend of the Ioffe–Regel parameter [26], which is a measure of the degree of disorder. Therefore this mechanism has the potential to increase the internal photon detection efficiency of an SSPD for the infrared photon wavelength range.

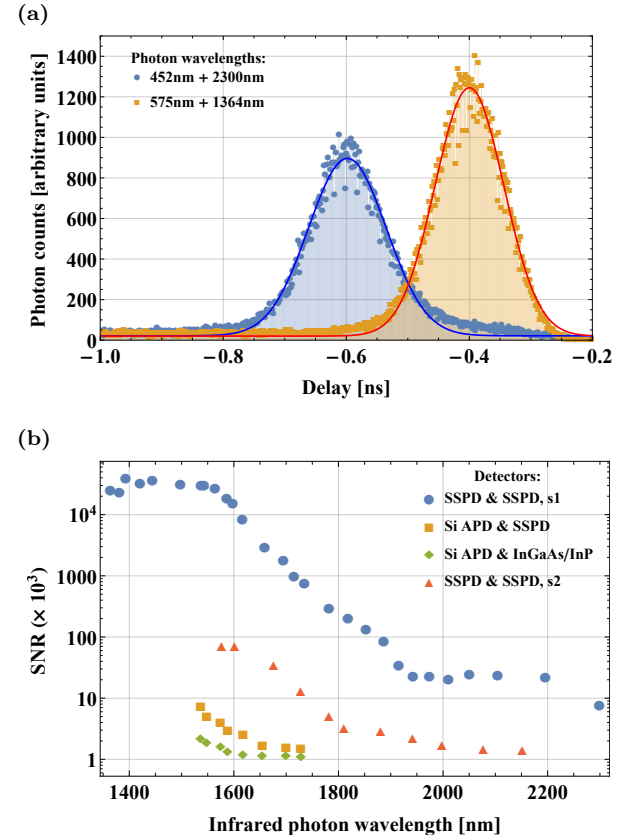


FIG. 5. (a) Arrival time coincidence histograms for two example settings. The measured setup timing jitter is approximately 86 ps (FWHM). (b) SNR for four different settings as described in the main text. Plot markers are bigger than error bars, excluding SNR values close to 1.

IV. CONCLUSION

Summarizing, we have developed the principles of the realization of the single photon receivers above telecom wavelength range based on NbN SSPD with high values of system detection efficiency. It was achieved by using more disordered NbN films. The best values of the system detection efficiency are: 60% at 1700 nm, 25% at 2000 nm, 15% at 2300 nm. Within the experimental scenario involving the entangled photons we have compared our SSPDs with other detectors. The best performance was achieved when using an SSPD/SSPD pair, which yielded at least three orders of magnitude better SNR as compared to the others. In this case the achieved values of the SNR were > 20000 up to 1600 nm, > 1000 in the wavelength range 1600 – 1700 nm, > 100 for 1700 – 1850 nm, and > 8 at around 1850 – 2300 nm.

V. FUNDING INFORMATION

PK and *MM* acknowledge support by:
- National Laboratory of Atomic, Molecular and Optical

Physics, Torun, Poland;

- Foundation for Polish Science (FNP) (project First Team co-financed by the European Union under the European Regional Development Fund);
- Ministry of Science and higher Education, Poland (MNiSW) (grant no. 6576/IA/SP/2016);

- National Science Centre, Poland (NCN) (Sonata 12 grant no. 2016/23/D/ST2/02064).

AD, YV, PM, KS, PZ acknowledge support by:

- the Russian Science Foundation (RSF) Project No. 18-12-00364.

- [1] F. Marsili, V. B. Verma, J. A. Stern, S. Harrington, A. E. Lita, T. Gerrits, I. Vayshenker, B. Baek, M. D. Shaw, R. P. Mirin, and S. W. Nam, *Nat. Photonics* **7**, 210 (2013).
- [2] V. B. Verma, B. Korzh, F. Bussières, R. D. Horansky, S. D. Dyer, A. E. Lita, I. Vayshenker, F. Marsili, M. D. Shaw, H. Zbinden, R. P. Mirin, and S. W. Nam, *Opt. Express* **23**, 33792 (2015).
- [3] I. Esmaeil Zadeh, J. W. Los, R. B. Gourgues, V. Steinmetz, G. Bulgarini, S. M. Dobrovolskiy, V. Zwiller, and S. N. Dorenbos, *APL Photonics* **2**, 111301 (2017).
- [4] W. Zhang, L. You, H. Li, J. Huang, C. Lv, L. Zhang, X. Liu, J. Wu, Z. Wang, and X. Xie, *Science China Physics, Mechanics & Astronomy* **60**, 120314 (2017).
- [5] K. Smirnov, A. Divochiy, Y. Vakhtomin, P. Morozov, P. Zolotov, A. Antipov, and V. Seleznev, *Superconductor Science and Technology* **31**, 035011 (2018).
- [6] V. Shcheslavskiy, P. Morozov, A. Divochiy, Y. Vakhtomin, K. Smirnov, and W. Becker, *Rev. Sci. Instrum.* **87**, 053117 (2016).
- [7] E. E. Wollman, V. B. Verma, A. D. Beyer, R. M. Briggs, B. Korzh, J. P. Allmaras, F. Marsili, A. E. Lita, R. P. Mirin, S. W. Nam, and M. D. Shaw, *Opt. Express* **25**, 26792 (2017).
- [8] G. Gol'tsman, O. Minaeva, A. Korneev, M. Tarkhov, I. Rubtsova, A. Divochiy, I. Milostnaya, G. Chulkova, N. Kaurova, B. Voronov, D. Pan, J. Kitaygorsky, A. Cross, A. Pearlman, I. Komissarov, W. Slysz, M. Wegezki, P. Grabiec, and R. Sobolewski, *IEEE Transactions on Applied Superconductivity* **17**, 246 (2007).
- [9] F. Marsili, F. Bellei, F. Najafi, A. E. Dane, E. A. Dauler, R. J. Molnar, and K. K. Berggren, *Nano Lett.* **12**, 4799 (2012).
- [10] L. Chen, D. Schwarzer, V. B. Verma, M. J. Stevens, F. Marsili, R. P. Mirin, S. W. Nam, and A. M. Wodtke, *Acc. Chem. Res.* **50**, 1400 (2017), <https://doi.org/10.1021/acs.accounts.7b00071>.
- [11] F. Marsili, V. Verma, M. J. Stevens, J. A. Stern, M. D. Shaw, A. Miller, D. Schwarzer, A. Wodtke, R. P. Mirin, and S. W. Nam, in *CLEO: 2013* (Optical Society of America, 2013) p. CTu1H.1.
- [12] D. Elvira, A. Michon, B. Fain, G. Patriarche, G. Beau-
doin, I. Robert-Philip, Y. Vakhtomin, A. V. Divochiy, K. V. Smirnov, G. N. Gol'tsman, I. Sagnes, and A. Beveratos, *Appl. Phys. Lett.* **97**, 131907 (2010), <https://doi.org/10.1063/1.3495985>.
- [13] K. Smirnov, A. Divochiy, Y. Vakhtomin, P. Morozov, P. Zolotov, A. Antipov, and V. Seleznev, *Supercond. Sci. Technol.* (2018).
- [14] P. I. Zolotov, A. V. Divochiy, Y. B. Vakhtomin, P. V. Morozov, V. A. Seleznev, and K. V. Smirnov, *J. Phys. Conf. Ser.* **917**, 062037 (2017).
- [15] <http://www.tydexoptics.com/>.
- [16] V. Anant, A. J. Kerman, E. A. Dauler, J. K. Yang, K. M. Rosfjord, and K. K. Berggren, *Opt Express* **16**, 10750 (2008).
- [17] S. N. Dorenbos, E. M. Reiger, N. Akopian, U. Perinetto, V. Zwiller, T. Zijlstra, and T. M. Klapwijk, *Applied Physics Letters* **93**, 161102 (2008), <https://doi.org/10.1063/1.3003579>.
- [18] S. Larouche and L. Martinu, *Appl Opt* **47**, C219 (2008).
- [19] A. Semenov, B. Günther, U. Böttger, H.-W. Hübers, H. Bartolf, A. Engel, A. Schilling, K. Ilin, M. Siegel, R. Schneider, D. Gerthsen, and N. A. Gippius, *Phys. Rev. B* **80**, 054510 (2009).
- [20] T. Lutz, P. Kolenderski, and T. Jennewein, *Opt. Lett.* **39**, 1481 (2014), arXiv:1309.4040.
- [21] M. Misiaszek, A. Gajewski, and P. Kolenderski, *Journal of Physics Communications* **2**, 065014 (2018), 1711.10232v1.
- [22] T. I. Baturina, A. Y. Mironov, V. M. Vinokur, M. R. Baklanov, and C. Strunk, *Phys. Rev. Lett.* **99**, 257003 (2007).
- [23] V. Gantmakher and V. T. Dolgopolov, *Physics - Uspekhi* **53**, 1 (2010).
- [24] S. P. Chockalingam, M. Chand, J. Jesudasan, V. Tripathi, and P. Raychaudhuri, *Phys. Rev. B* **77**, 214503 (2008).
- [25] S. P. Chockalingam, M. Chand, A. Kamlapure, J. Jesudasan, A. Mishra, V. Tripathi, and P. Raychaudhuri, *Phys. Rev. B* **79**, 094509 (2009).
- [26] D. Y. Vodolazov, *Phys. Rev. Applied* **7**, 034014 (2017).